Synthesis of Graphene Peroxide and Its Application in Fabricating Super Extensible and Highly Resilient Nanocomposite Hydrogels

Jiaqi Liu, Caifeng Chen, Changcheng He, Jing Zhao, Xiaojing Yang,* and Huiliang Wang*

College of Chemistry, Beijing Key Laboratory of Energy Conversion and Storage Materials, Beijing Normal University, Beijing 100875, People's Republic of China.

ABSTRACT

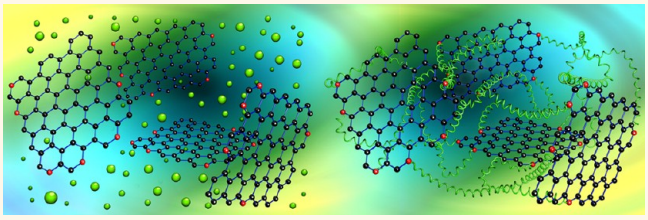

Functionalized graphene has been considered as one of the most important materials for preparing polymer nanocomposites due to its unique physical structure and properties. To increase the interfacial interaction between polymer component and graphene oxide (GO) sheets, *in situ* grafting polymerization initiated by a free radical initiator immobilized on GO sheets is a better choice. We report a facile and effective strategy for preparing graphene peroxide (GPO) *via* the radiation-induced peroxidation of GO. The formation of peroxides on GO is proven by iodometric measurement and other characterizations. Using GPO as a polyfunctional initiating and cross-linking center, we obtained GO composite hydrogels exhibiting excellent mechanical properties, namely, very high tensile strength (0.2−1.2 MPa), extremely high elongations (2000−5300%), and excellent resilience. This work provides new insight into the fabrication of GO/polymer nanocomposites to fulfill the excellent mechanical properties of graphene.

KEYWORDS: graphene · hydrogels · nanocomposites · elasticity · mechanical property

Graphene sheets have atomically thick two-dimensional structure and extraordinary electronic, thermal, and mechanical properties.[1−4] One of the most promising ways to exploit these properties for applications is to incorporate graphene or more often graphene oxide (GO) sheets into a polymer matrix.[5−9] Since graphene is proven to be one of the strongest but flexible materials ever tested,[2] the incorporation of graphene sheets as nanoscale fillers is expected to be able to significantly improve the mechanical properties of host polymers. Many efforts have been made to fabricate graphene-based polymer nanocomposites with enhanced mechanical properties.[5,10−12] However, the improvements are still inefficient, as reviewed by Macosko *et al.*[11] For the GO/polymer composites the improvements in tensile strength are usually less than 80%. Only for a few nanocomposites made with polymers (*e.g.*, polyvinyl alcohol) that can form strong hydrogen bonds with GO can the improvements be up to 100−300%.[13,14] The main reason is the lack of enough strong interactions between polymer chains and GO sheets. In most GO/polymer composites prepared by physical or chemical methods,[6] there are only weak physical interactions between GO sheets and polymer chains.

Undoubtedly, the introduction of strong covalent bonds by grafting would strongly increase the interfacial interaction between the polymer component and GO sheets.[6,15] The "grafting-to" approach utilizes the reactions between the reactive ends of a preformed polymer with the functional groups on GO.[16] However, it has some intrinsic drawbacks, *e.g.*, low-efficiency and the difficulty in obtaining a high grafting density. The "grafting-from" process, which involves the *in situ* polymerization initiated by the initiator covalently immobilized on GO sheets, is more effective in introducing high-density polymer chains. Several "grafting-from" methods have been developed in the last two years, such as atom transfer radical polymerization (ATRP),[15,17,18] reversible addition−fragmentation chain transfer (RAFT) polymerization,[19] *in situ* Ziegler−Natta polymerization,[20] and free radical polymerization (FRP).[21] Among them, ATRP is the most extensively studied method. However, these methods are usually multistep and difficult to control, and it is difficult to obtain

* Address correspondence to wanghl@bnu.edu.cn.

Received for review June 28, 2012 and accepted August 23, 2012.

Published online August 23, 2012
10.1021/nn302874v

high-molecular-weight polymers. Conventional FRP processes are commercially the most important and scientifically the most thoroughly investigated. The major reasons for this are that useful high-molecular-weight polymers and copolymers can be prepared from a wide variety of monomers; in addition, these processes are generally the easiest to carry out and control. Free radical initiators are usually required for the initiation of FRP. The most widely used initiators are compounds such as peroxides that easily decompose into two oxygen-centered radicals. If peroxides can be immobilized onto GO sheets, then the "grafting-from" approach can be performed with the convenient free radical grafting polymerization, and hence high-density grafted polymer chains with high molecular weight can be covalently attached to GO sheets. However, no reports on the peroxidation of graphene/GO and the grafting polymerization initiated by peroxides immobilized on graphene/GO sheets can be found yet.

Hydrogels are hydrophilic three-dimensional polymer networks that can absorb and retain a considerable amount of water with maintenance of shape. Research on hydrogels has been prompted by a number of potential applications in biomedical fields and a variety of other related potential uses.[22,23] So far, several GO/polymer composite hydrogels have been developed. For example, Shi *et al*. reported composite hydrogels made with GO and polyvinyl alcohol (PVA),[24] DNA,[25] and hemoglobin[26] by solution mixing; Liu *et al*. prepared a GO/PVA composite hydrogel with improved mechanical properties by solution mixing and freezing/thawing.[27] In these composite hydrogels, there is no strong chemical bonding between the polymer and GO sheets, even though for the GO/PVA composite hydrogels, strong physical cross-linking effect of PVA chains *via* hydrogen bonding is present. A few GO/polymer composite hydrogels with chemical bonding between the polymer and GO sheets are also reported.[28,29]

Most synthetic hydrogels are mechanically very weak, due to their intrinsic structural inhomogeneity and the lack of an energy-dissipation mechanism.[23,30] Improving the mechanical properties of the hydrogels is a prerequisite to broadening their applications, especially in biomedical fields, such as soft artificial tissues.[23,31] The development of hydrogels with novel microstructures and excellent mechanical properties is a fascinating and challenging topic in current gel research, and several tough hydrogels have been developed. Among them, double-network (DN)[32] and nanocomposite (NC)[33] gels are the most extensively studied. We have developed a strategy to fabricate tough hydrogels by using peroxidized macromolecular microspheres (MMSs)[34] or surfactant micelles[35] as polyfunctional initiating and cross-linking centers (PFICC). Since the long polymer chains are chemically attached to the uniformly distributed cross-linking centers, the gels exhibit very high compressive strengths (several to several tens of MPa).[34,35] If peroxides can be immobilized on graphene sheets, then the peroxidized graphene sheets can function as PFICC to produce high-density and long polymer chains covalently joined to them, and hence the obtained hydrogels may possess excellent mechanical properties.

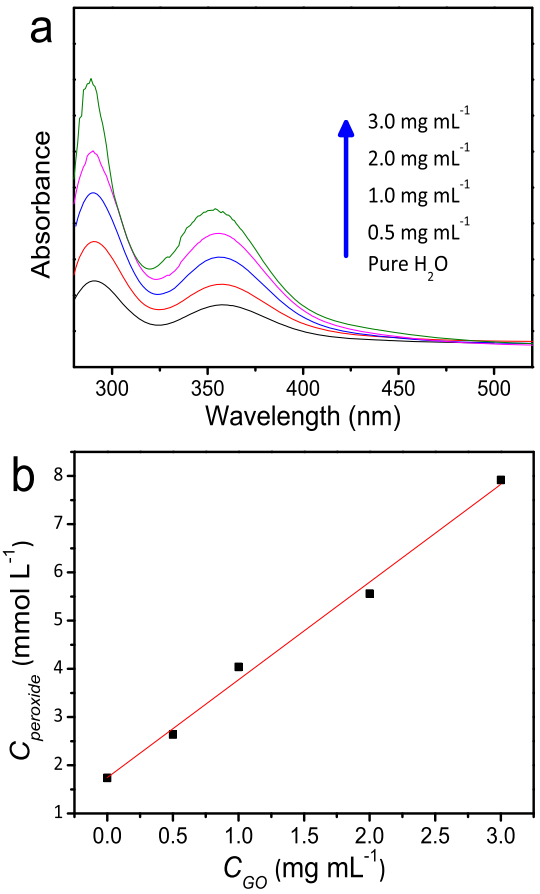

Figure 1. Iodometric measurement of peroxide formed in pure water and GO aqueous dispersions with different GO concentrations. (a) UV−visible spectra; (b) the concentration of peroxide ($C_{peroxide}$) as a function of GO concentration (C_{GO}).

In this article, we report for the first time the synthesis of graphene peroxide (GPO) and the fabrication of nanocomposite hydrogels by *in situ* free radical polymerization initiated by GPO. The obtained nanocomposite hydrogels exhibit excellent mechanical properties.

RESULTS AND DISCUSSION

We synthesized graphene peroxide with a simple radiation method, starting from graphene oxide that was prepared with the modified Hummers' method (Supporting Information).[36,37] The homogeneous well-exfoliated GO aqueous colloidal dispersions (Supporting Information, Figures S1 and S2) with different GO concentrations (0.5, 1.0, 2.0, and 3.0 mg mL^{-1}) were irradiated with ^{60}Co γ-rays for 12 h at a dose rate of 10 Gy min^{-1}. As a direct and reliable evidence for the formation of peroxide in the irradiated solutions, the classic iodometric

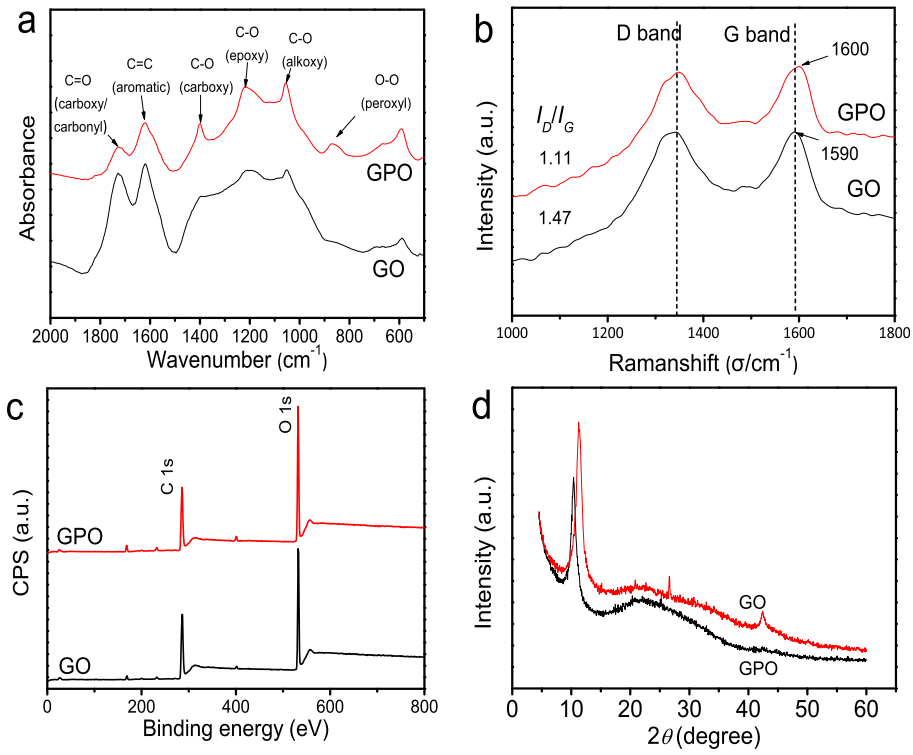

Figure 2. Evidence for the formation of GPO by the γ-radiation-induced peroxidation of GO. (a) FTIR, (b) Raman, (c) XPS, and (d) XRD spectra of GO and GPO.

TABLE 1. Absorbance Ratios of the Absorption Peaks to That of Aromatic C═C

	A_{1730}/A_{1618}	A_{1398}/A_{1618}	A_{1209}/A_{1618}	A_{1049}/A_{1618}
GO	0.96	0.03	0.09	0.19
GPO	0.78	0.67	0.57	0.72

method,[38] which utilizes the redox reaction of the peroxide with I^- to form I_2 (actually in the form of I_3^-), was employed to quantitatively determine the amount of peroxide. The UV−visible spectra of water and the GO aqueous dispersions after the treatment are shown in Figure 1a, and the characteristic absorption of I_3^- increased monotonically with the increase of GO concentration. The calculated concentrations of peroxide are shown in Figure 1b, and there is a linear relationship between the concentration of peroxide ($C_{peroxide}$) and the concentration of GO (C_{GO}). The value obtained by extrapolating the linear relationship to the C_{GO} of 0 (1.74 mmol L^{-1}) is exactly the same as that formed in pure water, with which a blank experiment was carried out. Therefore, the increased $C_{peroxide}$ in the GO dispersions is attributed to the peroxides formed on GO. From the slope of the linear line, the $C_{peroxide}$ formed on GO is about 2.0 mmol g^{-1}; that is, roughly 24 carbon atoms in every 1000 carbon atoms (2.4%) on GO are connected with peroxides. The iodometric measurements prove that peroxide has been formed on the GO.

Detailed characterizations of GPO were performed by comparison to GO. Both FTIR spectra of GO and GPO (Figure 2a) show the bands attributed to carboxy/carbonyl C═O (1730 cm^{-1}), aromatic C═C (1618 cm^{-1}), carboxy C−O (1398 cm^{-1}), epoxy C−O (1209 cm^{-1}), and alkoxy C−O (1049 cm^{-1}) stretches,[39] while a band attributed to a peroxy O−O (871 cm^{-1}) stretch[40] appeared in GPO, giving more direct evidence for the formation of peroxides on GO. In addition, a significant change in the intensities of some of the bands can also be found. For comparing the intensities of some bands, the bands are baseline subtracted to obtain their absorbance. Here we used the peak of aromatic C═C, which is more stable under high-energy irradiation, at 1618 cm^{-1} as an internal reference. The absorbance ratios of the absorption peaks to the reference peak (A/A_{1618}) are listed in Table 1. The absorbance ratio of carboxy/carbonyl C═O absorption decreases, while those of carboxy C−O, epoxy C−O, and alkoxy C−O absorptions increase.

The Raman spectra of GO and GPO are shown in Figure 2b. The D band indicates the size of the in-plane sp^2 domains, and the G band corresponds to the first-order scattering of the E_{2g} mode.[41] The G band of GPO is shifted to a higher frequency at about 1600 cm^{-1}, while that of GO is located at 1590 cm^{-1}. In addition, the Raman D/G intensity ratio (I_D/I_G) of GPO (1.11) decreases in comparison to that in GO (1.47). Since the I_D/I_G is proportional to the average size of the sp^2 domains,[41] the average size of the in-plane sp^2 domains in GPO actually decreases due to the irradiation process.

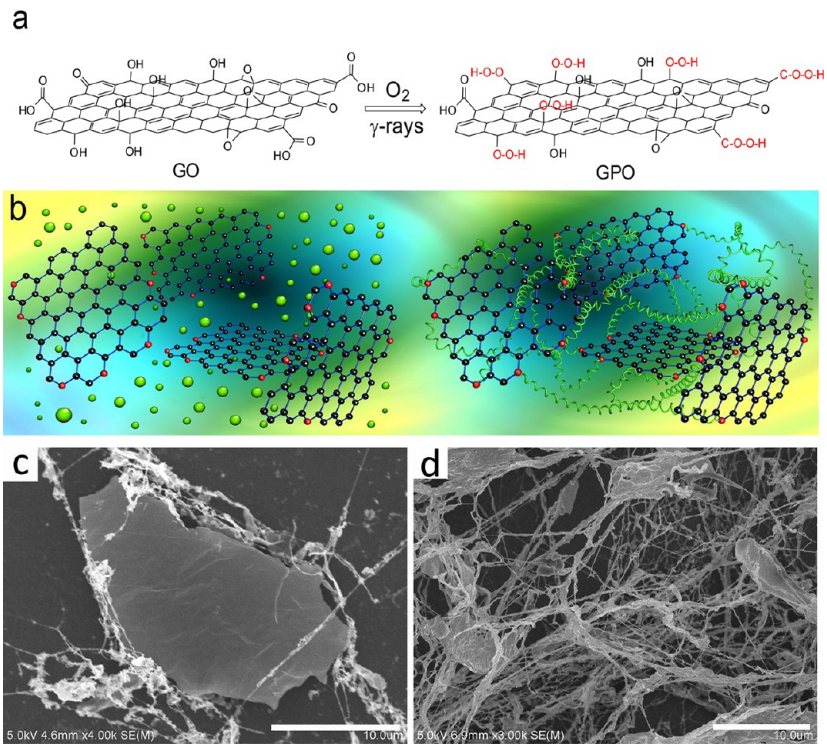

Figure 3. Mechanisms for the formation of GPO and a GPO hydrogel. (a) Possible schematic model of GO and GPO. (b) 3D schematic model for the formation of a GPO hydrogel, before (left side) and after (right side) polymerization. The green balls are the monomer molecules, the green spiral lines are the polymer chains, and the peroxyl groups are colored in red. (c, d) SEM micrographs showing the formation process of a GPO hydrogel; the reaction times were 6 min (c) and 12 min (d). Other reaction conditions: 2 mg mL^{-1} GPO concentration, 4 mol L^{-1} AAm concentration, and 45 °C reaction temperature. The reaction was stopped, and then the solution was diluted with 500 times deionized water. Scale bar: 10 μm.

The GO and GPO were also characterized by X-ray photoelectron spectrometry (XPS). The wide scan survey XPS spectra of GO and GPO (Figure 2c) show that the intensity ratio of O_{1s} to C_{1s} in GPO is increased in comparison to that in GO. The O/C atomic ratios calculated from the corresponding peak areas are 0.511 and 0.460 for GPO and GO, respectively, suggesting that GPO has a higher oxidation degree. The curve-fitting results of the C_{1s} peaks of GPO and GO (Supporting Information, Figure S3) also indicate that the percentage of alkoxy C increases but that of carbonyl/carboxyl C decreases. X-ray diffraction (XRD) analyses of GO and GPO were also carried out. As shown in Figure 2d, the XRD pattern of GPO shows a sharp diffraction peak at 2θ = 10.30°, which corresponds to a basal spacing of 0.85 nm, while those for GO are 11.32° and 0.78 nm. The increase of interlayer spacing in GPO is possibly due to the larger bond length of the peroxyl group (C−O−OH) and the presence of more water molecules in the interlayers.

The possible structure of GPO is shown in Figure 3a. Although the accurate structure of GO is still currently debated, most research indicates that hydroxyl and epoxy oxygen-based groups are present at a considerable concentration on the graphite basal plane, in addition to carbonyl and carboxyl groups on the periphery of the sheets.[42] Since the ^{60}Co γ-rays have a very high energy (1.25 MeV), the hydroxyl, epoxy, carbonyl, and carboxyl groups can be broken under irradiation to form radicals, which can combine with oxygen to form peroxy radicals. The peroxy radicals can further combine with a small radical, which might be formed by the radiolysis of water, to form peroxide.

From the FTIR and especially the XPS characterizations, it is reasonable to conclude that more oxygen-containing groups are formed on GPO, but only a small part of the functional groups on GO have been transformed into peroxides, since there are still a large number of these groups present in GPO (Figure 2a). The decreased absorbance ratio of carboxy/carbonyl C═O to aromatic C═C (Table 1) and the decreased atomic ratio of carbon in carboxy/carbonyl to nonoxygenated ring C from XPS analysis indicate that the carbonyl and carboxyl groups located at the edge of the GO sheets are easier to break under γ-ray irradiation to form peroxides. The possible reason is that the radicals formed at the edge under γ-ray irradiation are more unstable than those formed in the graphite basal plane, where the radicals can be stabilized by the hyperconjugation effect of the adjacent aromatic carbon double bonds.

The peroxides on GPO decompose on heating to generate free radicals (GO•, OH•), where GO•, the radicals on graphene, can initiate the grafting polymerization

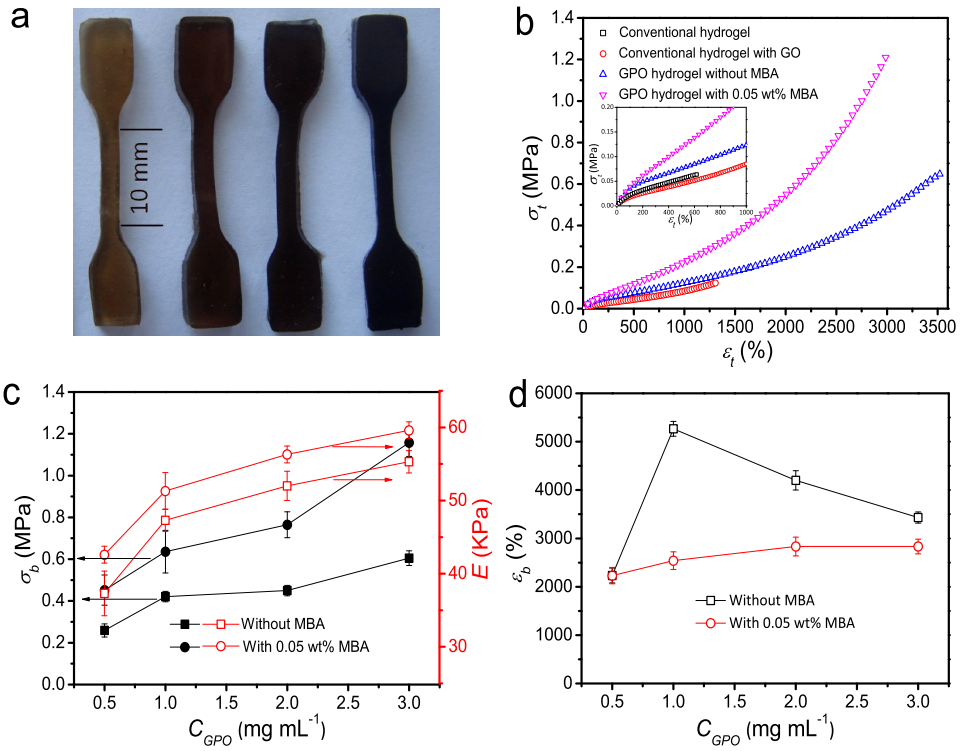

Figure 4. GPO hydrogels and their tensile mechanical properties. (a) Photograph of the dumbbell-shaped specimens made with GPO aqueous dispersions with different concentrations (from left to right: 0.5, 1.0, 2.0, and 3.0 mg mL^{-1}). (b) Stress−strain (σ_t−ε_t) curves of a conventional hydrogel, a conventional hydrogel with GO, and GPO hydrogels with or without MBA. The inset shows the σ_t−ε_t curves at low strains. GO and GPO concentrations were 3 mg mL^{-1}. (c, d) Fracture stress (σ_b) and elastic modulus (E) (c) and fracture strain (ε_b) (d) of the GPO hydrogels synthesized with different GPO concentrations with or without MBA. Reaction conditions: 4 mol L^{-1} AAm concentration, 45 °C reaction temperature. The water content of the gels was about 78 wt %.

of monomers onto the GPO sheets, and OH• can initiate homopolymerization of monomers. The growing grafted polymer chains on vicinal GPO sheets can be covalently joined through mutual combination and/or be physically entangled, *i.e.*, chemically and/or physically cross-linked (Figure 3b). Due to the presence of a larger number of peroxides on each GPO sheet, GPO sheets function as polyfunctional initiating and cross-linking centers. Such a formation mechanism and corresponding microstructure occurring in the GPO hydrogels is described here.

The GPO hydrogels could not be dissolved in a large excess of water even after immersion for one month, but instead reached equilibrium swelling (Supporting Information, Figure S4), indicating the presence of chemical cross-linking in the GPO hydrogels. A gel-like material could also be obtained using the irradiated water, in which the hydroperoxide formed functions as an initiator. However, it was completely dissolved upon immersion in water in less than 4 days, indicating little or no strong covalent interactions (*i.e.*, no chemical cross-linking) between the polymer chains. SEM investigations of the reaction mixture after different reaction times show that isolated GPO sheets are connected by long fibers (in micrometers) (Figure 3c), which are bundles of polymer chains. With the increase of reaction time, more and longer fibers are formed, and hence a three-dimensional network structure is formed (Figure 3d). It is interesting to find that the fibers more frequently start at the edges of the GPO sheets.

We fabricated a series of polyacrylamide (PAAm) hydrogels by using GPO aqueous dispersions with different GPO concentrations (C_{GPO}) as the PFICC. The obtained nanocomposite hydrogels are termed GPO hydrogels. To ensure the uniform dispersion of GPO, the highest C_{GPO} in this work was selected as 3 mg mL^{-1}. The color of the gels changed from brown to black with the increase of C_{GPO} (Figure 4a). The GPO hydrogels exhibit mechanical properties that are much improved over those of the conventional hydrogels. Figure 4b shows the typical stress−strain (σ_t−ε_t) curves of a GPO hydrogel and two conventional hydrogels, whose synthesis is described in the Supporting Information. The conventional gel without GO is the weakest one; its fracture tensile stress (σ_b) is only about 0.064 MPa, and its breaking tensile strain (ε_b) is about 630%. When GO is incorporated into the conventional gel, the σ_b and ε_b of the gel are both doubled, suggesting there are some interactions, possibly hydrogen bonding, between the GO sheets and the polymer chains. More impressively, the σ_b of the GPO hydrogel is about 0.65 MPa, and its ε_b is 3500%. In addition, the elastic modulus (E) of the GPO gel

(about 52 kPa) is also higher than that of the conventional gels (27 and 30 kPa). The GPO hydrogel shows mechanical improvements as high as 900% and 500% in σ_b and ε_b, respectively, in comparison to the conventional hydrogel without GO, indicating that the use of GPO as PFICC can dramatically improve the mechanical properties of hydrogels. The mechanical improvements in the GPO hydrogel are the highest reported.[5,10−12]

The σ_b, E, and ε_b of the GPO gels are summarized in Figure 4c, d. The σ_b and E steadily increase with increasing C_{GPO}, but ε_b decreases with C_{GPO} except for 0.5 mg mL^{-1}. The mechanical properties of GPO hydrogels are further improved by adding a very small amount of chemical cross-linker (<0.1 wt %, mass ratio to the monomer). The typical $\sigma_t-\varepsilon_t$ curve and the σ_b, E, and ε_b of the GPO hydrogels synthesized with 0.05% *N*,*N*′-methylenebisacrylamide (MBA) are also included in Figure 4b−d. Their σ_b and E also increase with increasing C_{GPO}, whereas ε_b stays almost constant. In comparison with the GPO hydrogels without MBA, the σ_b and E of the GPO hydrogels with MBA are significantly higher, but their ε_b's are lower.

Our GPO hydrogels exhibit excellent mechanical properties. In comparison to most extensively studied tough double-network[32] and nanocomposite[33] gels, the tensile strength of the GPO gels (0.2−1.2 MPa) is similar to that of DN gels (sub-MPa to several MPa) and is usually higher than that of NC gels (0.1−1 MPa); meanwhile, the extensibility of GPO gels (2000−5300%) is higher than most other tough gels (1000−3000%).[30] The extensibility of 5300% exhibited by the GPO gel with 0.1% GO is the highest even reported (Supporting Information, Figure S5).

Moreover, the GPO gels also exhibit excellent elastic recovery. Cyclic tensile tests were carried out on the hydrogels synthesized with or without MBA to a maximum tensile strain (ε_{max}) of 1600% for 8 cycles (Supporting Information, Movie S1). A hysteresis loop can be found only in the first loading−unloading cycle, and it became negligible in the following cycles (Figure 5a). The hysteresis ratios (h_r)[43] of each loading−unloading cycle number for the GPO gels stretched to different ε_{max} are shown in Figure 5b. The h_r of the GPO gel with MBA at each cycle to the same ε_{max} is always lower than that of GPO gel without MBA, and it decreases with decreasing ε_{max}. In the first cycle to ε_{max} = 1600%, the h_r's of the GPO gels with or without MBA are about 0.145 and 0.206, respectively. When ε_{max} = 800%, the h_r of the GPO gel with MBA is only 0.08, which is only about one-tenth that of a NC gel (up to 0.87) and is still much lower than that of a modified NC gel (0.19).[43] The h_r of the GPO gels in the following cycles are extremely low, *e.g.*, only 0.036 (ε_{max} = 1600%) for the gel without MBA and 0.006 for the gel with MBA (ε_{max} = 800%). Furthermore, the GPO gel without MBA has a low residual strain of about 50% after the 8 cycles, and the GPO gel with MBA has extremely low residual strains (<5%) after being

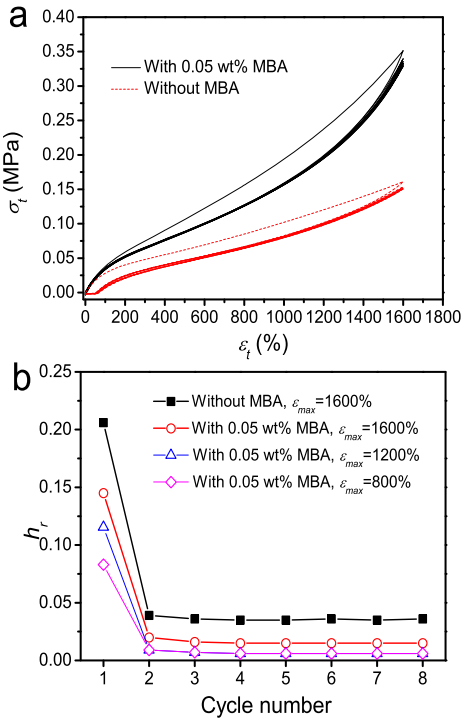

Figure 5. Resilience of the GPO hydrogels with or without MBA. (a) Cyclic tensile loading−unloading curves of the GPO gels to the strain of 1600% for 8 cycles. (b) Hysteresis ratios (h_r) of each cycle number for the GPO gels being stretched to different maximum tensile strains (ε_{max}). Reaction conditions: 3 mg mL^{-1} GPO concentration, 4 mol L^{-1} AAm concentration, water content of the samples ~78 wt %.

stretched to different ε_{max} and even to the fracture strain (Figure 5a and Supporting Information, Figure S6), suggesting the extraordinary resilience of the GPO gels. The phenomenon that a gel can completely recover to its original shape after being elongated to very high strains larger than 2500% has not been reported previously. As mentioned earlier, both DN and NC gels exhibit high mechanical strengths; however, they show poor resilience at a high strain, because of the breakage of the highly cross-linked first network[44] and the desorption of polymer chains from the clay sheets,[45] respectively.

Dynamic mechanical analysis measurement also reveals that the elastic (storage) modulus (E') of the GPO gel is always much higher than the viscous (loss) modulus (E'') over the tested range from 0.1 to 10 Hz (Figure 6), showing a bulk elastic response with slight dependence on the frequency (f). The small and stable loss factor (tan δ) indicates that the GPO hydrogels have a good elastic recovery property, in accordance with the tensile test results.

Increasing C_{GPO} has two important effects on the microstructure of the GPO hydrogels: (i) more but shorter grafted chains are formed due to the increase of peroxide concentration; (ii) the distance between GPO sheets becomes smaller, and therefore the grafted chains on vicinal sheets are more easily cross-linked. More grafted polymer chains on closer GPO sheets would

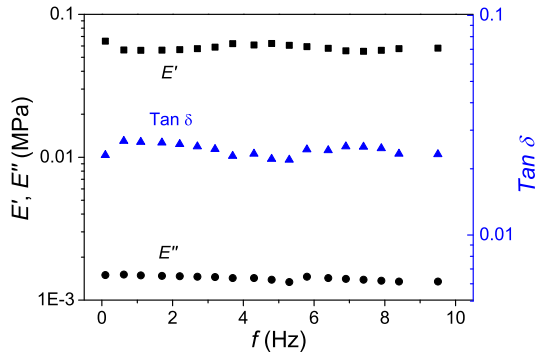

Figure 6. Storage modulus (E'), loss modulus (E''), and loss factor (tan δ) of a GPO gel as a function of frequency (f). Reaction conditions: 3 mg mL^{-1} GPO concentration, 4 mol L^{-1} AAm concentration, water content of the sample ~78 wt %.

lead to a larger number of active chains, which leads to a higher σ_b and E of the gels (Figure 4c), in accordance with rubber elasticity theory; however, on the other side, the shorter polymer chains between the GPO sheets imply a lower ε_b. The unusual low ε_b at C_{GPO} = 0.5 mg mL^{-1} (Figure 4d) is expected, as there are not enough active chains connecting GPO sheets.[35]

The introduction of MBA into the reaction solution reduces the proportion of dangling chains. In addition, some of the homopolymer chains might also be covalently joined to the grafted polymer chains, which increases the effective length of grafted polymer chains and hence their probability to become physically entangled. Both mechanisms increase the number of active chains. Therefore, the GPO hydrogels synthesized with the addition of a slight amount of MBA exhibited much improved mechanical properties because they recruit a larger number of chains during deformation.

CONCLUSIONS

In summary, this work demonstrates for the first time the synthesis of graphene peroxide and its application in fabricating superextensible and highly resilient graphene-based nanocomposite hydrogels. By irradiating the graphene oxide aqueous dispersion with γ-rays in the presence of oxygen, part of the functional groups on GO can be transformed into peroxides. By using the GPO as a polyfunctional initiating and cross-linking center, graphene-based composite hydrogels with exceptional mechanical properties are fabricated. The nanocomposite hydrogels show very high tensile strengths, medium elastic moduli, and extremely high elongations, in addition to very low hysteresis and excellent resilience. This work provides new insight into the fabrication of GO/polymer nanocomposites to fulfill the excellent mechanical properties of graphene. The nanocomposite hydrogels exhibit several up to 10 times improvements in tensile strength and fracture strain in comparison to conventional gels; the mechanical improvements are the highest reported for GO/polymer composites. The mechanical properties of the GPO gels are comparable to those of some soft tissues,[23] and hence these materials can be potentially applied as soft artificial tissues in biomedical fields and for the design of soft biomimetic machines.[46] Due to the versatility and convenience of radical polymerization initiated by peroxides, we believe that many types of polymer composites with unique microstructures and extraordinary mechanical properties can also be fabricated.

EXPERIMENTAL SECTION

Synthesis and Characterization of Graphene Peroxide. Graphite oxide used in this study was prepared according to the modified Hummers' method,[36] and the detailed synthesis procedure is described in the Supporting Information. GO was dispersed in deionized water by ultrasonication and mechanical stirring for 2 h at room temperature to obtain a GO aqueous colloidal dispersion. The GO aqueous colloidal dispersions with different GO concentrations (0.5, 1.0, 2.0, and 3.0 mg mL^{-1}) were irradiated with ^{60}Co γ-rays for 12 h at a dose rate of 10 Gy min^{-1}. To ensure the continuous supply of oxygen, the solutions were bubbled with oxygen (50 mL min^{-1}) during the irradiation process. For comparison, pure water was also irradiated in the same way. The irradiated dispersions and water were kept at 4–5 °C in a refrigerator to prevent thermal decomposition of the peroxides.

The concentrations of peroxide formed in the irradiated GPO colloidal dispersions and pure water were measured by the classical iodometric method.[38] The concentration of I_3^- formed was measured at 360 nm with a TU-1901 UV–vis spectrometer (Pgeneral, China). The molar extinction coefficient for I_3^- at 360 nm is 25 000 L mol^{-1} cm^{-1}.

The irradiated GPO dispersions were freeze-dried with a FD-1B-50 vacuum freeze-dryer (Beijing Boyikang Laboratory Apparatus Co., Ltd., China) to obtain dry GPO sheets for the following characterizations. Dry GO sheets were also obtained and characterized. Fourier-transform infrared (FTIR) spectra of the samples were recorded on a Nicolet-380 FTIR spectrometer (USA) using the KBr method in the range 400–3600 cm^{-1}. Raman spectra were measured from 200 to 3000 cm^{-1} on a microscopic confocal Raman spectrometer (LavRAM Aramis, Horiba Jobin Yvon, France), using a 633 nm He–Ne laser. XPS data were taken on an AXIS-Ultra instrument from Kratos Analytical (Shimadzu, Japan) using monochromatic Al Kα radiation (225 W, 15 mA, 15 kV) and low-energy electron flooding for charge compensation. To compensate for surface charge effects, binding energies were calibrated using a C_{1s} hydrocarbon peak at 284.80 eV. Composition of the surface of a thin film can be inferred from the relative peak area. XRD analyses of freeze-dried GPO and GO were performed by using a D8 Advance X-ray diffractometer with Cu Kα radiation in the 2θ range 4–60° (PANalytical, The Netherlands).

Preparation of GPO Hydrogels. A 2.843 g sample of acrylamide (AAm, ultrapure, BioDev, Japan) was dissolved in 10 mL of GPO aqueous dispersions with different GPO concentrations (0.5, 1.0, 2.0, and 3.0 mg mL^{-1}), respectively. Here we used the original concentration of GO as the concentration of GPO. The well-dispersed systems were transferred to glass molds made by placing a silicone spacer with a height of 2 mm between two flat glass plates. Then the systems were deaerated with bubbling nitrogen for 30 min. After being sealed, the samples were placed in a water bath at 45 °C for 36 h, where they formed hydrogels.

SEM Investigation of the Formation Process of the GPO Hydrogels. To investigate the formation process of the GPO hydrogel, the polymerization reaction was stopped after a very short time by

quickly cooling the solution and adding ethanol. A 20 μL solution was extracted and then diluted with 10 mL of deionized water. The solution was rapidly plunged into liquid nitrogen for about 5 min and then freeze-dried until all water was removed. The freeze-dried sample was placed on a silicon wafer and then investigated with scanning electron microscopy (SEM) (S-4800, Hitachi, Japan).

Mechanical Tests of GPO Hydrogels. For uniaxial tensile tests dumbbell-shaped specimens cut according to DIN-53504 S3 (overall length: 35 mm; width: 6 mm; inner width: 2 mm, gauge length: 10 mm, thickness: 2 mm) were tested with an Instron 3366 electronic universal testing machine (Instron Corporation, MA, USA) at a crosshead speed of 40 mm min^{-1}. The tensile stress (σ_t) was calculated as follows. σ_t = Load/tw (t and w were the initial thickness and width of the dumbbell-shaped gel sample, respectively). The tensile strain (ε_t) is defined as the change in the length relative to the initial gauge length, and the breaking tensile strain (ε_b) is the tensile strain at which the sample breaks. Stress and strain between ε_t = 10−30% were used to calculate the initial elastic modulus (E). At least three specimens per experimental point were tested in all mechanical measurements to obtain reliable values. Cyclic tests were performed by performing subsequent trials immediately following the initial loading with the same specimen at a crosshead speed of 160 mm min^{-1}. The gel specimens were coated with a thin layer of silicon oil to prevent the evaporation of water during the tests. Oscillating compression tests were performed on the cylindrical hydrogels with a diameter of 20 mm and a height of 10 mm at room temperature with a dynamic mechanical analyzer (Q800, TA Instruments, USA). The gels were placed in between two metal parallel plates and lubricated with dodecane to prevent drying and barreling. Each sample was preloaded to 0.01 N, which was followed by a multifrequency sweep in the range 0.1−10 Hz to a strain of 5%.

Conflict of Interest: The authors declare no competing financial interest.

Acknowledgment. We appreciate financial support from the National Science Foundation of China (Nos. 50673013, 21074014, and 50872012), the Fundamental Research Funds for the Central Universities, and Beijing Municipal Commission of Education. We thank Prof. Hugh R. Brown and Dr. Phillip Whitten of University of Wollongong, Australia, for commenting on the manuscript.

Supporting Information Available: Additional Experimental Section, Figures S1−S6, and supporting Movie S1. This material is available free of charge *via* the Internet at http://pubs.acs.org.

REFERENCES AND NOTES

1. Geim, A. K. Graphene: Status and Prospects. *Science* **2009**, *324*, 1530–1534.
2. Lee, C.; Wei, X. D.; Kysar, J. W.; Hone, J. Measurement of the Elastic Properties and Intrinsic Strength of Monolayer Graphene. *Science* **2008**, *321*, 385–388.
3. Suk, J. W.; Piner, R. D.; An, J. H.; Ruoff, R. S. Mechanical Properties of Mono Layer Graphene Oxide. *ACS Nano* **2010**, *4*, 6557–6564.
4. Seol, J. H.; Jo, I.; Moore, A. L.; Lindsay, L.; Aitken, Z. H.; Pettes, M. T.; Li, X. S.; Yao, Z.; Huang, R.; Broido, D.; *et al*. Two-Dimensional Phonon Transport in Supported Graphene. *Science* **2010**, *328*, 213–216.
5. Stankovich, S.; Dikin, D. A.; Dommett, G. H. B.; Kohlhaas, K. M.; Zimney, E. J.; Stach, E. A.; Piner, R. D.; Nguyen, S. T.; Ruoff, R. S. Graphene-Based Composite Materials. *Nature* **2006**, *442*, 282–286.
6. Bai, H.; Li, C.; Shi, G. Q. Functional Composite Materials Based on Chemically Converted Graphene. *Adv. Mater.* **2011**, *23*, 1089–1115.
7. Zhu, Y. W.; Murali, S.; Cai, W. W.; Li, X. S.; Suk, J. W.; Potts, J. R.; Ruoff, R. S. Graphene and Graphene Oxide: Synthesis, Properties, and Applications. *Adv. Mater.* **2010**, *22*, 3906–3924.
8. Liang, J. J.; Huang, Y.; Zhang, L.; Wang, Y.; Ma, Y. F.; Guo, T. Y.; Chen, Y. S. Molecular-Level Dispersion of Graphene into Poly(Vinyl Alcohol) and Effective Reinforcement of their Nanocomposites. *Adv. Funct. Mater.* **2009**, *19*, 2297–2302.
9. Tang, H. X.; Ehlert, G. J.; Lin, Y. R.; Sodano, H. A. Highly Efficient Synthesis of Graphene Nanocomposites. *Nano Lett.* **2012**, *12*, 84–90.
10. Potts, J. R.; Dreyer, D. R.; Bielawski, C. W.; Ruoff, R. S. Graphene-Based Polymer Nanocomposites. *Polymer* **2011**, *52*, 5–25.
11. Kim, H.; Abdala, A. A.; Macosko, C. W. Graphene/Polymer Nanocomposites. *Macromolecules* **2010**, *43*, 6515–6530.
12. Sengupta, R.; Bhattacharya, M.; Bandyopadhyay, S.; Bhowmick, A. K. A Review on the Mechanical and Electrical Properties of Graphite and Modified Graphite Reinforced Polymer Composites. *Prog. Polym. Sci.* **2011**, *36*, 638–670.
13. Zhao, X.; Zhang, Q.; Chen, D.; Lu, P. Enhanced Mechanical Properties of Graphene-Based Poly(Vinyl Alcohol) Composites. *Macromolecules* **2010**, *43*, 2357–2363.
14. Shen, J.; Yan, B.; Li, T.; Long, Y.; Li, N.; Ye, M. Mechanical, Thermal and Swelling Properties of Poly(acrylic acid)-Graphene Oxide Composite Hydrogels. *Soft Matter* **2012**, *8*, 1831–1836.
15. Salavagione, H. J.; Martínez, G.; Ellis, G. Recent Advances in the Covalent Modification of Graphene with Polymers. *Macromol. Rapid Commun.* **2011**, *32*, 1771–1789.
16. Mohamadi, S.; Sharifi-Sanjani, N.; Mahdavi, H. Functionalization of Graphene Sheets *via* Chemically Grafting of PMMA Chains Through *in-situ* Polymerization. *J. Macromol. Sci., Pure Appl. Chem.* **2011**, *48*, 577–582.
17. Ren, L.; Huang, S.; Zhang, C.; Wang, R.; Tjiu, W.; Liu, T. Functionalization of Graphene and Grafting of Temperature-Responsive Surfaces from Graphene by ATRP "on Water". *J. Nanopart. Res.* **2012**, *14*, 1–9.
18. Fang, M.; Wang, K.; Lu, H.; Yang, Y.; Nutt, S. Covalent Polymer Functionalization of Graphene Nanosheets and Mechanical Properties of Composites. *J. Mater. Chem.* **2009**, *19*, 7098–7105.
19. Liu, J.; Tao, L.; Yang, W.; Li, D.; Boyer, C.; Wuhrer, R.; Braet, F.; Davis, T. P. Synthesis, Characterization, and Multilayer Assembly of pH Sensitive Graphene-Polymer Nanocomposites. *Langmuir* **2010**, *26*, 10068–10075.
20. Huang, Y.; Qin, Y.; Zhou, Y.; Niu, H.; Yu, Z.-Z.; Dong, J.-Y. Polypropylene/Graphene Oxide Nanocomposites Prepared by *in Situ* Ziegler-Natta Polymerization. *Chem. Mater.* **2010**, *22*, 4096–4102.
21. Kan, L.; Xu, Z.; Gao, C. General Avenue to Individually Dispersed Graphene Oxide-Based Two-Dimensional Molecular Brushes by Free Radical Polymerization. *Macromolecules* **2010**, *44*, 444–452.
22. Peppas, N. A.; Hilt, J. Z.; Khademhosseini, A.; Langer, R. Hydrogels in Biology and Medicine: From Molecular Principles to Bionanotechnology. *Adv. Mater.* **2006**, *18*, 1345–1360.
23. Gong, J. P.; Osada, Y. Soft and Wet Materials: From Hydrogels to Biotissues. *Adv. Polym. Sci.* **2010**, *236*, 203–246.
24. Bai, H.; Li, C.; Wang, X. L.; Shi, G. Q. A pH-Sensitive Graphene Oxide Composite Hydrogel. *Chem. Commun.* **2010**, *46*, 2376–2378.
25. Xu, Y. X.; Wu, Q. O.; Sun, Y. Q.; Bai, H.; Shi, G. Q. Three-Dimensional Self-Assembly of Graphene Oxide and DNA into Multifunctional Hydrogels. *ACS Nano* **2010**, *4*, 7358–7362.
26. Huang, C. C.; Bai, H.; Li, C.; Shi, G. Q. A Graphene Oxide/Hemoglobin Composite Hydrogel for Enzymatic Catalysis in Organic Solvents. *Chem. Commun.* **2011**, *47*, 4962–4964.
27. Zhang, L.; Wang, Z. P.; Xu, C.; Li, Y.; Gao, J. P.; Wang, W.; Liu, Y. High Strength Graphene Oxide/Polyvinyl Alcohol Composite Hydrogels. *J. Mater. Chem.* **2011**, *21*, 10399–10406.
28. Sun, S. T.; Wu, P. Y. A One-Step Strategy for Thermal- and pH-Responsive Graphene Oxide Interpenetrating Polymer Hydrogel Networks. *J. Mater. Chem.* **2011**, *21*, 4095–4097.
29. Zhang, N. N.; Li, R. Q.; Zhang, L.; Chen, H. B.; Wang, W. C.; Liu, Y.; Wu, T.; Wang, X. D.; Wang, W.; Li, Y.; *et al*. Actuator Materials Based on Graphene Oxide/Polyacrylamide Composite Hydrogels Prepared by *in Situ* Polymerization. *Soft Matter* **2011**, *7*, 7231–7239.

30. Naficy, S.; Brown, H. R.; Razal, J. M.; Spinks, G. M.; Whitten, P. G. Progress Toward Robust Polymer Hydrogels. *Aust. J. Chem.* **2011**, *64*, 1007–1025.
31. Tanaka, Y.; Gong, J. P.; Osada, Y. Novel Hydrogels with Excellent Mechanical Performance. *Prog. Polym. Sci.* **2005**, *30*, 1–9.
32. Gong, J. P.; Katsuyama, Y.; Kurokawa, T.; Osada, Y. Double-Network Hydrogels with Extremely High Mechanical Strength. *Adv. Mater.* **2003**, *15*, 1155–1158.
33. Haraguchi, K.; Takehisa, T. Nanocomposite Hydrogels: A Unique Organic-Inorganic Network Structure with Extraordinary Mechanical, Optical, and Swelling/Deswelling Properties. *Adv. Mater.* **2002**, *14*, 1120–1124.
34. Huang, T.; Xu, H. G.; Jiao, K. X.; Zhu, L. P.; Brown, H. R.; Wang, H. L. A Novel Hydrogel with High Mechanical Strength: A Macromolecular Microsphere Composite Hydrogel. *Adv. Mater.* **2007**, *19*, 1622–1627.
35. He, C. C.; Jiao, K. X.; Zhang, X.; Xiang, M.; Li, Z. Y.; Wang, H. L. Nanoparticles, Microgels and Bulk Hydrogels with Very High Mechanical Strength Starting from Micelles. *Soft Matter* **2011**, *7*, 2943–2952.
36. Hummers, W. S.; Offeman, R. E. Preparation of Graphitic Oxide. *J. Am. Chem. Soc.* **1958**, *80*, 1339–1339.
37. Liu, Z. H.; Wang, Z. M.; Yang, X. J.; Ooi, K. Intercalation of Organic Ammonium Ions into Layered Graphite Oxide. *Langmuir* **2002**, *18*, 4926–4932.
38. Štefanić, I.; LaVerne, J. A. Temperature Dependence of the Hydrogen Peroxide Production in the γ-Radiolysis of Water. *J. Phys. Chem. A* **2001**, *106*, 447–452.
39. Park, S.; Dikin, D. A.; Nguyen, S. T.; Ruoff, R. S. Graphene Oxide Sheets Chemically Cross-Linked by Polyallylamine. *J. Phys. Chem. C* **2009**, *113*, 15801–15804.
40. Vacque, V.; Sombret, B.; Huvenne, J. P.; Legrand, P.; Suc, S. Characterisation of the O-O Peroxide Bond by Vibrational Spectroscopy. *Spectrochim. Acta A* **1997**, *53*, 55–66.
41. Kudin, K. N.; Ozbas, B.; Schniepp, H. C.; Prud'homme, R. K.; Aksay, I. A.; Car, R. Raman Spectra of Graphite Oxide and Functionalized Graphene Sheets. *Nano Lett.* **2008**, *8*, 36–41.
42. Dreyer, D. R.; Park, S.; Bielawski, C. W.; Ruoff, R. S. The Chemistry of Graphene Oxide. *Chem. Soc. Rev.* **2010**, *39*, 228–240.
43. Zhu, M.; Liu, Y.; Sun, B.; Zhang, W.; Liu, X.; Yu, H.; Zhang, Y.; Kuckling, D.; Adler, H.-J. P. A Novel Highly Resilient Nanocomposite Hydrogel with Low Hysteresis and Ultrahigh Elongation. *Macromol. Rapid Commun.* **2006**, *27*, 1023–1028.
44. Webber, R. E.; Creton, C.; Brown, H. R.; Gong, J. P. Large Strain Hysteresis and Mullins Effect of Tough Double-Network Hydrogels. *Macromolecules* **2007**, *40*, 2919–2927.
45. Nishida, T.; Endo, H.; Osaka, N.; Li, H.-j.; Haraguchi, K.; Shibayama, M. Deformation Mechanism of Nanocomposite Gels Studied by Contrast Variation Small-Angle Neutron Scattering. *Phys. Rev. E* **2009**, *80*, 030801.
46. Calvert, P. Hydrogels for Soft Machines. *Adv. Mater.* **2009**, *21*, 743–756.